Using hybrid functionals to investigate MoS_2 and adsorbed organic molecules.

Rémi Lierdeman
EPFL supervisor : Nicola Marzari
Local supervisors : Ronaldo Pela, Ignacio Gonzalez
Group director : Claudia Draxl

April 2021

Contents

1 Introduction

Two dimensional Transition metal dichalcogenide (TMDCs) semiconductors offer promising applications for ultra thin optoelectronic applications that could not be performed with semi-metallic graphene[2]. Monolayer MoS_2 is one of those particularly promising TMDCs as it has a direct band gap in the visible range[9][14]. In the research of new interesting materials obtained with these substrates, Hybrid inorganic/organic structures are very exciting as they can combine charge carrier properties from the inorganic substrate[14] and light sensitivity of organic molecules[33, 32]. From the interface, can also emerge properties found in neither of the components[5]. Good understanding of these electronic properties requires in depth investigation of what happens at the electronic scale. In this regard, hybrid systems raise a challenge as methods proven efficient for describing the inorganic substrate might be unfit for the organic molecules and inversely. In this intent, density functional theory (DFT) based methods provide quality insight onto the electronic structure[5][27].
Methods within and beyond DFT offer very helpful computational method to study the electronic structure and properties of many body systems like molecules or condensed matter. It has become a standard for quantum computations[15].
The fundamental idea of DFT is to replace a multi-electronic wave function, the main ingredient in a many-body problem, by the electronic density[15]. This fact combined with the progress of computational power in the last decades led to the possibility to investigate complex structures with up to thousands of atoms[16]. One relevant property, the total energy, is computed through the use of exchange-correlation functionals of the electrons density. These functionals can be improved from the most simple local density approximation (LDA)to the general gradient approximation (GGA), or even beyond DFT by introducing the exact Hartree-Fock (HF) exchange method[5].

In this project, we employ GGA and Hybrid functionals to investigate the electronic properties of monolayer MoS_2 with adsorbed pyridine and pyrene. The thesis is divided as follows: in section 2, we provide the theoretical background for this work. In section 3, explain the methodological framework used to obtain our results. In section 4, we show and discuss our results. Section 5 is dedicated to present additional works that could not be achieved successfully and an outlook for future works. And finally, we summarize the thesis with our conclusions

2 Theoretical background

2.1 Fundamentals of Density Functional Theory

The basis of Density Functional Theory relies on Hohneberg-Kohn's theorems which can be phrased as follows :

- When considering an electrons gas under the influence of an external potential, there exists a unique relationship between the groundstate density of charge and the external potential. Hence, the physical quantities such as the total energy can be expressed as functionals of the external potential. As a consequence of the bi-univocity between the external potential and the density of charges ($V_{ext} \leftrightarrow n(\mathbf{r})$), physical quantities such as the total energy of the

groundstate are also a unique functionals of the groundstate electronic density :

$$E = E[n(\mathbf{r})] \tag{1}$$

- The second theorem is a variational principle applied to a functional of the electronic density. It states that there exists a universal functional of the electronic density $n(\mathbf{r})$ describing the energy of the system $E[n(\mathbf{r})]$. Such that, for a given potential and number of electrons, the minimal value of this functional is the ground state of the system and the corresponding density $n_0(\mathbf{r})$ is the density of the ground state :

$$\frac{\delta E[n(\mathbf{r})]}{\delta n(\mathbf{r})}|_{n_0(\mathbf{r})} = 0 \tag{2}$$

The kinetic energy of an electron gas being unknown, Walter Kohn and Lu Sham suggested to replace the interacting electrons system by a problem of independent electrons in an external potential in the energy functional.

$$E_S[n] = T_S[n] + V_S[n] \tag{3}$$

Where $T_S[n]$ is the kinetic energy of non-interacting electrons, and $V_S[n]$ the potential that includes the external potential as well as the electron-electron interaction potential. This reformulation leads to a system of self consistent equations to be solved, known as the Kohn-Sham equations :

$$(-\frac{\nabla^2}{2m} + v_{eff})\phi_i = \epsilon_i \phi_i \tag{4}$$

with :

$$v_e ff(\mathbf{r}) = v_{ext}(\mathbf{r}) + e^2 \int \frac{\rho(\mathbf{r})}{|\mathbf{r} - \mathbf{r'}|} d\mathbf{r'} + \frac{\delta E_{xc}[\rho]}{\delta \rho(\mathbf{r})} \tag{5}$$

Where the first term is the external potential, the second one is the Coulomb energy, and the last one the exchange-correlation (xc) potential. This last parameter is detailed later.

2.2 Local density approximation (LDA)

The local density approximation is the most simple class of exchange-correlation energy functional, as it relies only on the value of the electronic density through space. It is expressed as :

$$E_{xc}^{LDA}[n] = \int n(\mathbf{r}) \epsilon_{xc}(n(\mathbf{r})) d\mathbf{r} \tag{6}$$

Where ϵ_{xc} is the exchange-correlation energy for one particle in an homogeneous gas of density n. The exchange contribution (E_x^{LDA}) is obtained by the homogeneous electron gas (HEG) model where the charges are assumed to be evenly distributed in space : $E_x^{LDA} = -\frac{3}{4}(\frac{3}{\pi})^{\frac{1}{3}} \int \rho(\mathbf{r})^{\frac{4}{3}} d\mathbf{r}$. The correlation part that measures the mutual influence of electrons can be computed by different approaches[6, 29, 31].

2.3 Generalized gradients approximation (GGA)

The Perdew-Burke-Ernzerhof (PBE) functional, is a type of generalized gradients approximation (GGA) functional. These approximations are improvement of the local density approximation (LDA) that considers an electron gas, and assumes a uniform electronic density. In GGAs, we consider the inhomogeneity of real systems, and their spatial variations in the expression of the energy functional. The general exchange-correlation energy of GGA approximations is generally defined as :

$$E_{xc}^{GGA}[n] = \int n(\mathbf{r})\epsilon_{xc}[n, \nabla n] \tag{7}$$

Where ϵ_{xc} now depends on the density and the density gradient. Further improvement can be made by including the laplacian of the density (the so called meta-GGA functionals), but it is not studied here.

2.4 Hybrid functionals

2.4.1 PBE0

The PBE0 hybrid functional introduces the Hartree-Fock exact exchange functional to the PBE functional exchange, and the total energy of PBE0 is written as follows:

$$E_{xc}^{PBE0} = \alpha E_x^{HF} + (1-\alpha)E_x^{PBE} + E_c^{PBE} \tag{8}$$

Where E_x^{HF} is the exchange term as given by the Hartree-Fock approach, E_x^{PBE} is the exchange term as given by the PBE functional, and E_c^{PBE} is the correlation as given by PBE.
The mixing parameter α, a crucial parameter for the accuracy of PBE0 as it determines which proportion of the exchange Energy is obtained by the Hartree-Fock method. It has been established in the literature that a value of $\alpha \simeq 0.25$ should provide the most accurate for many materials[4], however this parameter can be modified and optimized using solely the electronic density[25].

2.4.2 HSE

The HSE (Heyd, Scuseria, Ernzerhof) Hybrid functional introduces an error function screened Coulomb potential to the H-F exchange contribution of the PBE0 functional. This screening is said to improve the computational efficiency while giving an accuracy comparable to PBE0. The principle behind the efficiency gain is to compute the expensive exact H-F method only on a short range, and to use the less expensive E_x^{PBE} for long range interactions. The expression for the exchange-correlation energy within HSE is :

$$E_{xc}^{HSE,\omega} = \alpha E_x^{HF,SR}(\omega) + (1-\alpha)E_x^{PBE,SR}(\omega) + E_x^{PBE,LR}(\omega) + E_c^{PBE} \tag{9}$$

Where SR and LR show respectively the short range and long range coulomb corrections, and the parameter ω controls the "range length" of the Coulomb screening.
The Coulomb operator is split between SR and LR as follow :

$$\frac{1}{r} = \frac{erf(\omega r)}{r} + \frac{erfc(\omega r)}{r} \tag{10}$$

2.5 The `exciting` code

The `exciting` code is an all-electron full-potential DFT code which uses linearized augmented plane waves (LAPW) and local-orbitals as basis set[1].
Here we explain how this is achieved.

2.5.1 LAPW + lo

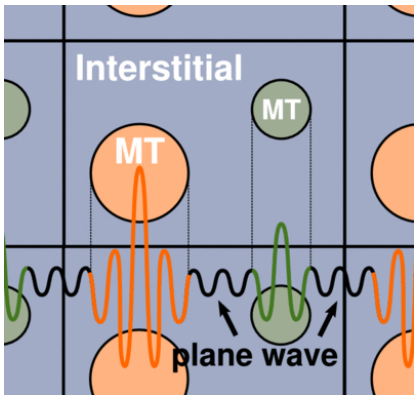

Figure 1: 2D representation of the partition of real space for augmented plane waves[23]

APW : The main idea behind Augmented Plane Wave (APW), is to separate the space between non-overlapping muffin-tin regions (spheres) containing the core electrons and interstitial regions figure.1. This partition determines the basis set to expand the KS wave functions :

$$\psi_{i\mathbf{k}}(\mathbf{r}) = \sum_{\mathbf{G}} C_{i\mathbf{G}} \phi_{\mathbf{G}+\mathbf{k}}(\mathbf{r}) \tag{11}$$

Where the functions are summed over the reciprocal lattice vectors $\mathbf{G}$.
In the interstitial region, the basis functions $\phi_{\mathbf{G}+\mathbf{k}}(\mathbf{r})$ are plane waves :

$$\phi_{\mathbf{G}+\mathbf{k}}(\mathbf{r}) = \frac{1}{\sqrt{\Omega}} e^{i(\mathbf{G}+\mathbf{k})\mathbf{r}} \tag{12}$$

And in the muffin-tin regions, the plane waves are augmented by the atomic-like functions, i.e. a set of spherical harmonics $Y_l^m(\mathbf{r})$ and radial functions u_l :

$$\phi_{\mathbf{G}+\mathbf{k}}(\mathbf{r}) = \sum_{lm} A_{lm\alpha}^{\mathbf{G}+\mathbf{k}\alpha} u_{l\alpha}(r_\alpha, E) Y_{lm}(\mathbf{r}) \tag{13}$$

Where α indexes the next neighboring nucleus, and $\mathbf{r}_\alpha$ the position relative to the nucleus $\mathbf{r}_\alpha = \mathbf{r} - \mathbf{R}_\alpha$.
So, unlike pseudo-potential methods, the electrons are not simply separated between core electrons and valence electrons, we end up having : core electrons confined in the muffin-tin region and solved by the Dirac equation (full relativity), semi-core electrons localized but not strictly confined to the MT region, and delocalized valence electrons.

However, the APW has some drawbacks, this is a non-linear eigenvalue problem and thus can not be solved in a single shot, the basis set has the energy as a variational parameter.
Linearization : These problems can be solved by linearizing these equations with respect to the energy. In this sense, a term containing the energy derivative is added to the basis functions :

$$\phi_{\mathbf{G+k}}(\mathbf{r}) = \sum_{lm}(A_{lm\alpha}^{\mathbf{G+k}\alpha} u_{l\alpha}(r_\alpha, E_l) + B_{lm\alpha}^{\mathbf{G+k}\alpha} \dot{u}_{l\alpha}(r_\alpha, E_l))Y_{lm}(\mathbf{r}) \tag{14}$$

This method has the advantage of being full potential, however, E_l has to be fixed thus, there is only one principal quantum number per l and thus is not "all-electron".
The eigenvalue problem now reads like :

$$\sum_{\mathbf{G'}}(H_{\mathbf{k+G,k+G'}} - \epsilon_{n\mathbf{k}} S_{\mathbf{k+G,k+G'}})C_{n\mathbf{k}}(\mathbf{G'}) = 0 \tag{15}$$

With H the Kohn-Sham hamiltonian and $S_{\mathbf{k+G,k+G'}} =< \phi_{G+k}|\phi_{G'+k} >$ the overlap matrix.

A drawback is that the derivative parameter introduces a distortion in the basis functions inside the MT, and we need more basis functions to correct them and achieve the same behavior as in APW.
(L)APW + lo An alternative way to linearize the APW basis set with fixed energy, is by introducing the local orbitals basis functions :

$$\phi_\mu(\mathbf{r}) = \begin{cases} \delta_{\alpha\alpha_\mu}\delta_{ll_\mu}\delta_{mm_\mu}[a_\mu u_{l\alpha}(r_\alpha;\epsilon_{l\alpha}) + b_\mu \dot{u}_{l\alpha}(r_\alpha;\epsilon_{l\alpha})]Y_{lm}(\vec{r_\alpha}), & r_\alpha \leq R_{MT} \\ 0, & \mathbf{r} \in I \end{cases} \tag{16}$$

Filling the boundary conditions of continuity at the border of the muffin tin region, and $\int_\Omega |\phi_\mu(\mathbf{r})|^2 d\mathbf{r} = 1$. This method allows us to have both the full potential of LAPW, and all-electrons considered thanks to the local-orbitals basis set.

3 Methodology

3.1 Hybrid Inorganic Organic System

Similar HIOS computations have been made with the `exciting` code on bulk Zinc oxyde and chemisorbed pyridine[27]. Here we investigated a different kind of adsorption, as the adhesion is made through weak Van-der-Waals forces between monolayer MoS_2 and pyridine and pyrene molecules.

In heterostructures, the level alignment is essential for optoelectronic applications[3]. MoS_2 has a strong carrier mobility and the organic molecules have a strong light-matter coupling, a type-I level alignment would make a potential light-emitting device, and a type-II alignment could be used for solar cells[3, 32, 27, 33]. And as it is important, the determination of the alignment type is also a delicate problem as small quantitative errors can lead to qualitatively incorrect descriptions[5].

3.1.1 Monolayer MoS_2

Molybdenum disulfide (MoS_2) belongs to the Transition metal dichalcogenide monolayers (TMDC) class of materials, i.e it is a 2D semiconductor of type MX_2 (wth M a transition metal, and X a

chalcogene),the Molybdenum layer is in between two layers of Sulfur, in an hexagonal structure. each Mo atom is thus bonded to 6 sulfide ions (fig 2). Bulk TMDCs are made of stacked layers of TMDCs bound by Van-der-Waals forces like graphite.
Bulk MoS_2 has on indirect bandgap $\simeq$ 1.2eV, between K and Γ, and when the number of layers decreases, the bandagap becomes direct and localized on K, and increases to $\simeq$ 1.89 eV for the optical bandgap[11], estimation of the electronic bandgap have been made using photocurrent spectroscopy[9] and found $\simeq$ 2.4.

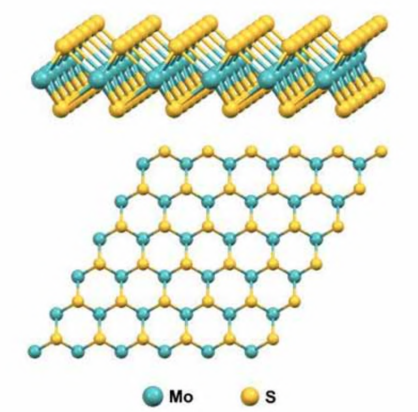

Figure 2: MoS_2 crystalline structure[12]

There exists different metastable crystalline phases of MoS2 fig 3, in this project, we exclusively focused on monolayer hexagonal MoS_2, so it is assumed (unless said otherwise), that every time we mention MoS_2, we are talking about this phase.

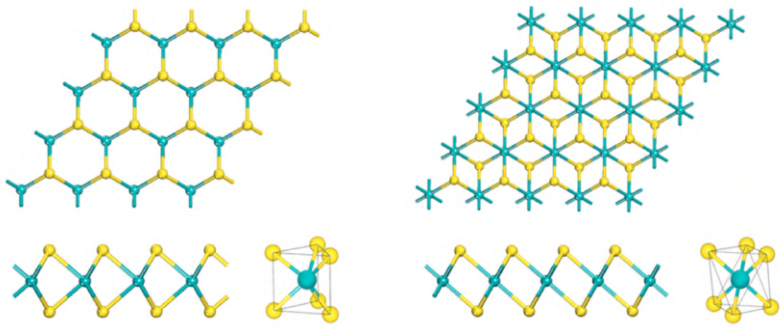

Figure 3: MoS_2 can have different crystalline phases, on the left the 2H (Hexagonal symmetry) (that we used for these computations), and the 3R(Rhombohedral symmetry) phase on the right[34]

3.1.2 Pyridine

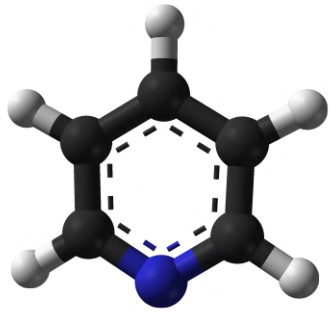

Figure 4: Representation of a pyridine molecule[26]

Pyridine (C_5H_5) is a small heterocyclic organic molecule (fig 4) very similar to benzene with one CH group replaced by a nitrogen atom. The molecule has an aromatic ring of 6 π electrons delocalized around the ring. The presence of the nitrogen in the ring provides a lone pair as a sp^2 orbital.
Pyridines molecules have an HOMO-LUMO gap $\simeq$ 6.12eV[8]. Due to its aromaticity, pyridine molecules are particularly stable, the presence of the Nitrogen atom makes it slightly electron deficient, it lowers the "π electron donor-acceptor" parameter[28]
This molecule also allows functionalization[24] which could provide further applications.

The computations of pyridine @ MoS_2 were all made on 2x2 MoS_2 supercells with adsorbed pyridine, these are quite small cells, and that means there is probably minor electronic interferences between neighboring cells pyridine molecules, but making the computations on bigger MoS_2 supercells would have been more time consuming.

3.1.3 Pyrene

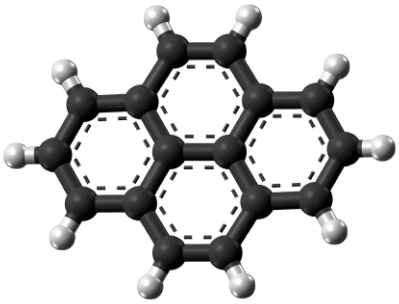

Figure 5: Representation of a pyrene molecule[22]

The pyrene molecule ($C_{16}H_{10}$) fig.5 is an aromatic system made of four carbon rings with a HOMO-LUMO gap $\simeq 5.7eV$[13]. Pyrene is a strong donor and can be used for light harvesting applications[33]. So with this material, we can expect a type-II alignment with the HOMO located higher than the substrate's valence band.

The pyrene molecule being bigger, we performed the computations on a 3x3 MoS_2 supercell, the system being bigger, the hybrid computations took way longer (almost a month), so we could not perform as many experiments as we did with the 2x2 MoS_2 and pyridine system.

3.2 Convergence tests

To provide quantitatively accurate results, we had to converge a certain input parameters.

3.2.1 rgkmax

The parameter rgkmax is crucial for running LAPW+lo calculations as it determines the size of the basis set. This dimensionless parameter is defined as the product of the smallest muffin-tin radius of the system $R_{MT,Min}$ and $|\mathbf{G}+\mathbf{K}|_{max}$, the maximum value of $\mathbf{G}+\mathbf{K}$, as each $\mathbf{G}+\mathbf{K}$ vector represents one basis function, rgkmax indirectly gives the number of basis functions to solve the Kohn-Sham equations. Typical rgkmax values of 5 and 7 are required for atoms with p and d orbitals respectively[1]. As our systems contains Hydrogen atoms with small muffin-tin radii of 1 Bohr, a small rgkmax value should be sufficient.

Table 1: convergence of the rgkmax parameter using local density approximation, the convergence can be considered reached around 3.5

rgkmax	3	3.5	3.7	4	4.5
Bandgap (eV)	1.7487	1.7477	1.7476	1.7474	1.7473

Since the hybrid functional computations are really computationally expensive, a first convergence was made using a fast LDA method 1 and estimated a rgkmax around 3.5, this was later confirmed by a convergence on HSE computations 2. We kept these values for both systems (2x2 MoS_2/Pyridine and 3x3 MoS_2/Pyrene), as they are qualitatively quite similar and contain the same atoms with the same muffin-tin values.

Table 2: Convergence of the rgkmax parameter using the general gradients approximation, the convergence can be considered reached around 3.5 as predicted by the LDA

rgkmax	3	3.5	3.6
Bandgap (eV)	1.7489	1.7484	1.7484

3.2.2 Grid size

DFT computations also need to be converged on the k-grid, indeed, the basis functions are computed on a subset of k-points belonging to the primitive cell. As we are studying a 2D material, the subset does not need to be expanded on the G_3 axis, and since the direct band gap is located on $\vec{K} = 1/3\vec{G_1} + 1/3\vec{G_2}$, the subset of k-points should be of the form (3n , 3n , 1). The computational cost being directly related to the number of k points.

Table 3: Convergence of the subset of k-points over the four smallest multiples of 3, the change in the band-gap is very small, and it is safe to take the smallest (3, 3, 1) k-grid.

rgkmax	3x3x1	6x6x1	9x9x1	1x12x1
Bandgap (eV)	1.748	1.750	1.750	1.749

On figure3, we see that the variations in the band gap are $\simeq 10^{-3}$, and it is sufficient to work on the 3x3x1 k-grid.

3.2.3 Number of empty bands

In the exciting code, the integer parameter nempty corresponds to the number of empty eigenstates above the charge neutrality.
While this number is not really important for standard DFT computations, as it only gives the number of conduction bands computed, it is decisive for hybrid functionals because it determines the matrix size for the H-F contribution. This parameter needs to be converged for each system, however it is safe to assume that the convergence for PBE0 functional is also valid for HSE, as only the range of the H-F contribution differs.

Table 4: Convergence of the number of empty bands for pyridine @ 2x2 MoS_2, the change in the band-gap is very small after 50 so we consider this value for future reference.

Number of empty states	20	50	100	200
Bandgap (eV)	2.027	2.153	2.162	2.177

Table 5: Convergence of the number of empty bands for pyrene @ 3x3 MoS_2, the change in the band-gap is very small after 100 so we consider this value for future reference.

Number of empty states	60	80	100	120
Bandgap (eV)	1.311	1.448	1.527	1.545

The convergence can be seen on table 5 and table 4. The number of empty bands to be considered is directly related to the size of the system, we can consider the convergence reached for a pyridine @ 2x2 MoS_2 structure at 50 empty bands. For a pyrene @ 3x3 MoS_2 structure, the system is bigger

and requires a minimum of 100 empty states to have a marginal error.
We used these values for future computations for both PBE0 and HSE for the rest of the project.

4 Results

In this section, we present the results obtained in the project and their physical interpretations. We start with convergence tests on rgkmax, k-points, number of empty states. Then we proceed comparing electronic properties of pyridine @ MoS_2 and pyrene @ MoS_2 obtained with PBE, HSE and PBE0.

4.1 Pristine MoS_2 and molecules

Before starting any computation on heterostructures, we wanted to observe the computed results of our different functionals (PBE, PBE0 and HSE) on pristine monolayer MoS_2 crystal and single pyridine and pyrene molecules.

Experimental results of monolayer MoS_2 give a direct optical bandgap of 1.9 eV and an estimated electronic bandgap around 2.5 eV [11, 9]. As we can see on fig.6, PBE tends to slightly underestimate the bandgap and the hybrid functionals give more accurate result.

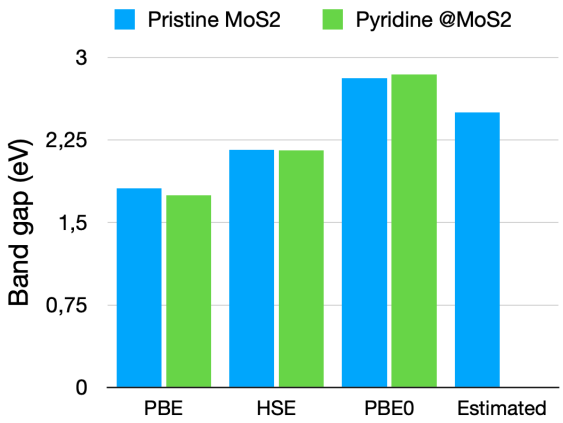

Figure 6: Bandgaps of pristine MoS_2 and pyridine @ MoS_2 using different functionals, compared with the photocurrent spectroscopy estimation.

The computation of a pyridine molecule shows again that PBE functional tends to really underestimate the electronic bandgap in particular for large gap materials. The H-F correction from hybrid functionals seems to give way mmore accurate results fig.7.

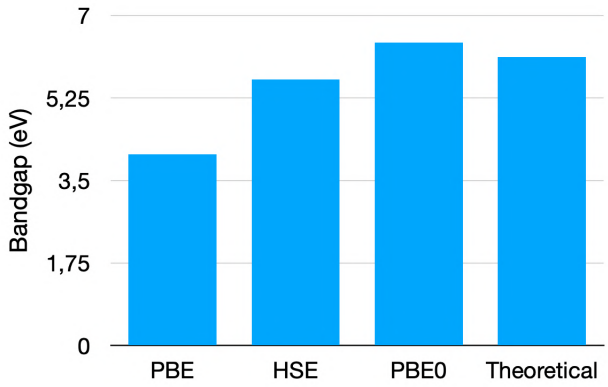

Figure 7: HOMO-LUMO gap of pyridine molecule using different functionals, compared to the estimated gap [8]

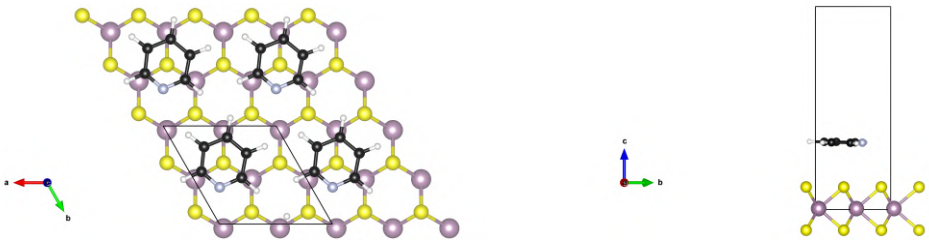

(a) $\vec{z}$ view (b) Side view

Figure 8: Representations of pyridine @ (2x2) MoS_2 supercells

4.2 Heterostructures

In this section we consider the results obtained for heterostructures, for that we look at the band structures and density of states graphs of the different materials. The interaction between the substrate and the adsorbed molecules being purely Van-der-Waals bound, no charge is transferred between the subsystems. We expect the band structure to be a superposition of the subsystems band structures. We are truly interested in what type of level alignment we have for these superpositions.

4.2.1 pyridine @ MoS_2

In figure11, we show the band structures of pyridine @ MoS_2 obtained with PBE, HSE and PBE0. Each band was projected onto the atoms, in red we plotted the lines projections on MoS_2 atoms, in black, the projections on carbon atoms, and in blue the bands projections on the nitrogen atom.

In the figure.11, we see that despite the quantitative variations of the band gap, qualitatively, all the functionals show a direct band gap coming from MoS_2 located at K point like pristine MoS_2. In figure6, we can see that the MoS_2 band gap is barely affected by the presence of the organic molecule, this is likely due to the absence of covalent bond between the two components, rather Vand-der-Waals interactions.

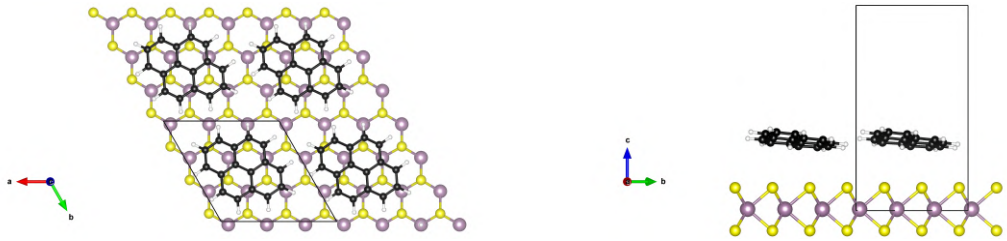

(a) $\vec{z}$ view (b) Side view

Figure 9: Representations of pyrene @ (3x3) MoS_2 supercells

More importantly, all the functionals find a type-I level alignment.
In figure12), we provide the density of states (DOS), considering PBE, HSE and PBE0. In the DOS, it is more evident that we have a type-I alignment. For HSE and PBE0, the offset between the HOMO and the top of valence bands are respectively 1.3 and 1.2 eV. The offset between the LUMO and the lowest conduction band is respectively 2.3 and 2.4. The size of the offsets strengthens the idea that we have a type-I alignment, as any quantitative error smaller than 1.2 eV would qualitatively not affect the alignment type, and HSE is said to provide an accuracy of the offset for heterojunctions smaller than 1 eV[7]. This conclusion and the fact that the band gap is in the visible range support that the heterostructure pyridine @ MoS_2 is a potential material for light emitting devices.

4.2.2 Pyrene @ MoS_2

As mentionned before, because of computational costs, only the PBE and HSE computations (with standards value $\alpha = 0.25$ and $\omega = 0.11 a_0^{-1}$) were made.

Folded band structure : The first thing we notice when observing the bandstructures fig.14 is the localization of the MoS_2 band gap, the theory tells us (and it was confirmed by previous computations) that the direct band gap of monolayer MoS_2 should be located on K, and here, we see it delocalized on Γ. This is actually not a computational error, it comes from the band folding, a recurring issue when computing supercells of a crystal. Indeed, when we consider for instance a 3x3 supercell, the reciprocal primitive cell would be 3x3 times smaller, and the bands inside this cell would be a superposition of neighboring primitive cell with an overlap distance $\frac{\mathbf{G}}{3}$ fig.21, in the previous case of the 2x2 supercell, the band gap was still located on K because $K = (\frac{1}{3}, \frac{1}{3}, 0) = (\frac{1}{3} - 0.5, \frac{1}{3}, 0) = (\frac{1}{3}, \frac{1}{3} - 0.5, 0)...$, but in the case of a 3x3 supercell, it folds the band gap to Γ. We notice also that the plot shows more bands for the same reason. But more of the band folding and unfolding is discussed in the outlook section.

Type-II alignment : On the band structures, as well as on the DOS figures, we also clearly see the HOMO of the pyrene molecule clearly above the MoS_2 valence bands. This corresponds to our expectations, considering that the pyrene is a strong electron donor[33]. This is qualitatively observed for both PBE and HSE computations, although quantitavely, the DOS of the HOMO is smaller with the PBE functional. This gives us a type-II alignment, which would make pyrene @

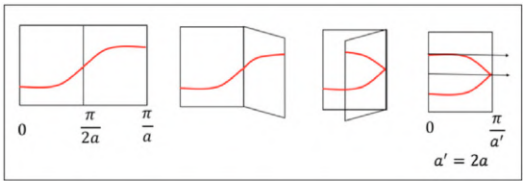

Figure 10: Folding band structure of a simplified 2x 1D supercell

MoS_2 a good light harvesting material. The offset between the HOMO and the highest valence band of MoS_2 is around 0.7/0.8 eV, so any quantitative error below that does not affect the alignment type, and HSE gives this precision[7].

This conclusion supports that the heterostructure pyrene @ MoS_2 is a potential material for light harvesting devices.

Polarity of MoS_2 : Pyrene is very sensitive to the polarity of its environment, it is even used as a probe to determine solvent environment[35]. MoS_2 is a polar material with strong spin-orbit coupling, and a spin orbit splitting of hundreds of meV[30], however for computational costs reasons, we entirely neglected the spin-orbit coupling of the systems for all the computations. DFT offers the possibility for any kind of functional to consider the system as a 2-body system (one for each spin) and compute with the polarity of the system. This should be a very interesting step for further investigations.

4.3 GGA vs Hybrid functionals

Before varying the various parameters of our hybrid functionals, we start by comparing the results obtained with a GGA functional (PBE), PBE0 and HSE ($\omega = 0.11a_0^{-1}$, $\alpha = 0.25$).

We previously observed that PBE functional tends to slightly underestimate the bandgap of MoS_2 and underestimate even more the HOMO-LUMO gap of Pyridine, on fig.**??**, 12, we can see the locations of HOMO and LUMO are even closer, it seems that the exchange energy provided by this method yields some sort of overlapping between the pyridine orbitals and the surface sulfur electrons, this is particularly visible on the band structures fig.12.
This tends to confirm that the exchange energy that takes a big role in non-covalent bondings is greatly undervalued by the exchange part of PBE computations, and it becomes really important when we study such heterojunctions to introduce an exact exchange component. The band structures given by the hybrid functionals on the other hand, leave the band structures of each material almost not affected by the other one, as one would expect for a non covalent junction.

4.4 From PBE0 to HSE (ω variation)

In figures 15and 16 we computed 2x2 MoS_2 supercells with adsorbed pyridine with different values of ω, as we can see, a decreased screening length (increased ω) leads to slightly smaller bandgaps, which means the long range exchange interactions play a non negligible role in the electronic structure. However it is interesting to notice, even with important screening parameters, namely

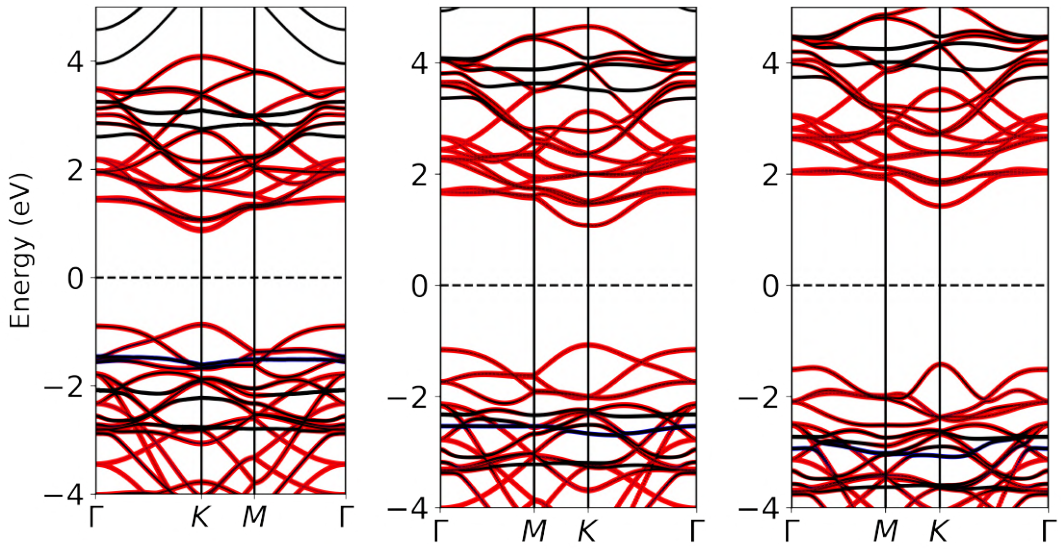

(a) PBE (b) HSE (c) PBE0

Figure 11: Comparison of the band structures for PBE functional and hybrid functionals of pyridine @ MoS_2

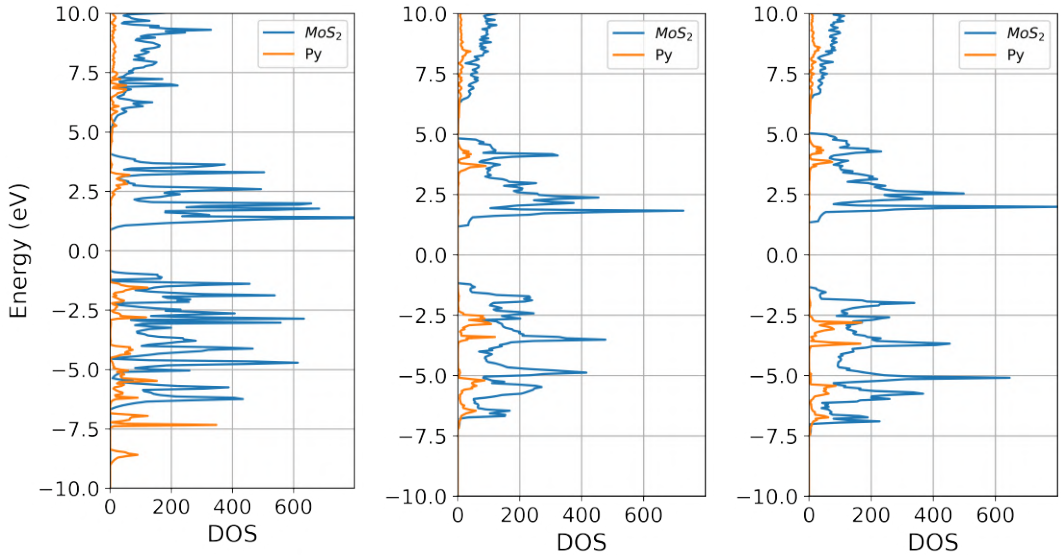

(a) PBE (b) HSE (c) PBE0

Figure 12: Comparison of the DOS for GGA(PBE) functionals and hybrid functionals of pyridine @ MoS_2

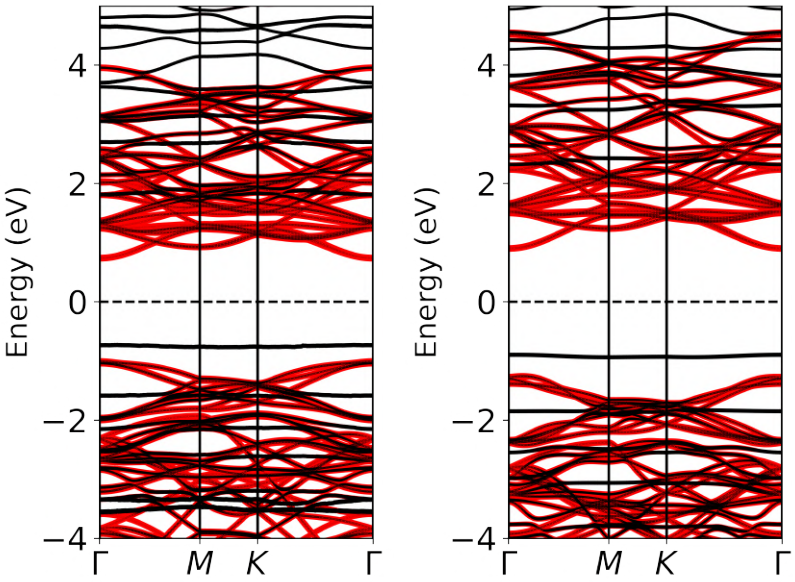

(a) PBE (b) HSE

Figure 13: Band structures for MoS_2 with adsorbed pyrene with PBE functional and HSE functional, the direct band gap is now located in Γ in the folded supercell

($\omega = 0.20a_0^{-1} \rightarrow$ screening length = 2.6Å), we don't observe the overlapping phenomenons we had with PBE functionals fig.**??**(a).
Since the distance between the molecule and the substrate is $\simeq 3.4$Å, It would be recommended to chose a screening parameter that gives a screening length $r = \frac{1}{\omega}$ larger than this distance[**?**].

4.5 Influence of the exchange parameter α

After observing the influence of the screening parameter on the hybrid, we consider the influence of the mixing parameter α, these two parameters should be considered together[17].
In figures 17 and 18, we plotted the band structures for $\alpha = 0.25; 0.5; 0.75$, ($\alpha = 0$ corresponds to a PBE computation).
We can see that increasing the alpha value noticeably increases the value of the electronic band gap of the MoS_2. But more important, it dramatically increases the HOMO-LUMO gap (stability of the pyridine molecule).
This can be explained by the fact that the H-F exchange parameter calculations systematically overestimate the charge transfer between bonded atoms due to lack of Coulomb electron correlation in the one-electron density and thus overestimates the aromaticity of cyclic organic molecules[10].
When we study this kind of system, it becomes really important to consider the perfect mixing parameter, and by experience, it is usually located around 0.25[10].

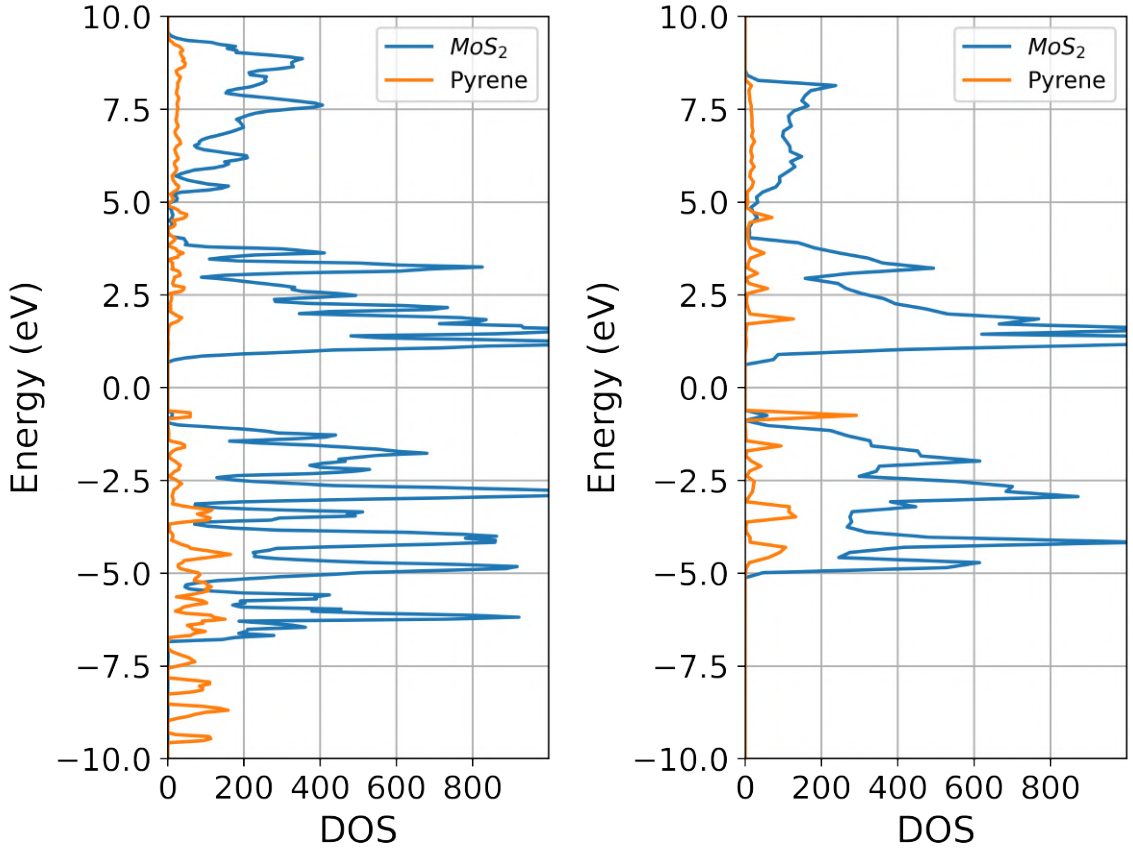

(a) PBE

(b) HSE

Figure 14: DOS for MoS_2 with adsorbed pyrene with GGA(PBE) functional and HSE functional, the direct band gap is now located in Γ in the folded supercell

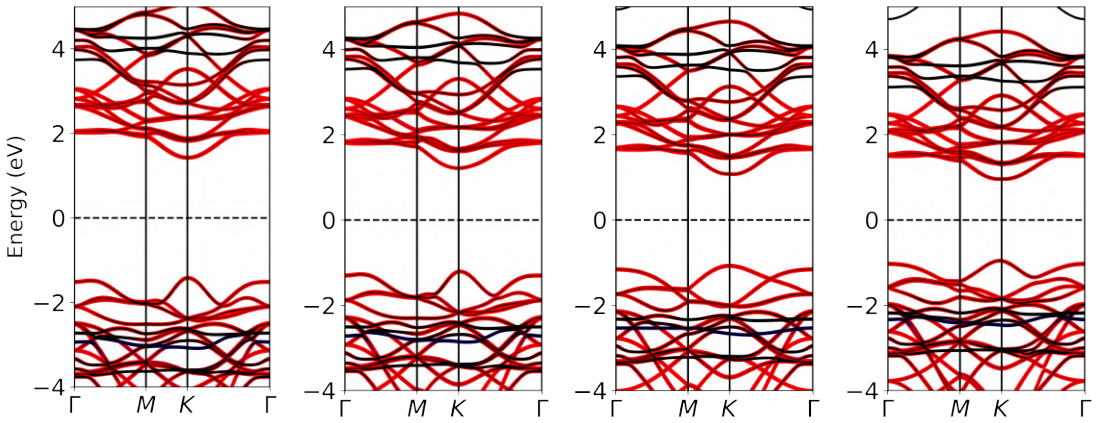

(a) $\omega = 0$ (PBE0) (b) $\omega = 0.05a_0^{-1}$ (c) $\omega = 0.11a_0^{-1}$ (d) $\omega = 0.20a_0^{-1}$

Figure 15: Band structures of MoS_2 / pyridine with varying ω

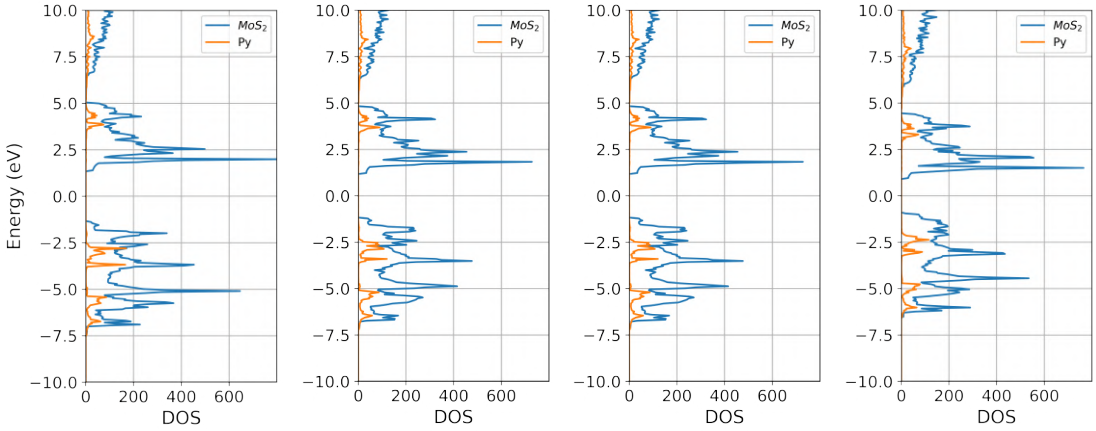

(a) $\omega = 0.0$ (PBE0) (b) $\omega = 0.05a_0^{-1}$ (c) $\omega = 0.11a_0^{-1}$ (d) $\omega = 0.20a_0^{-1}$

Figure 16: DOS of MoS_2 and adsorbed pyridine with varying ω parameter

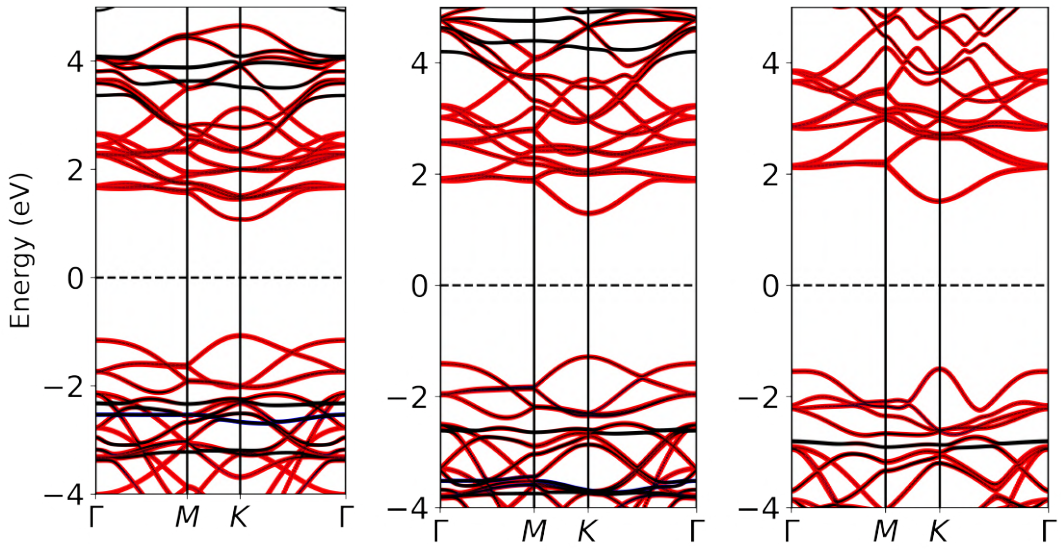

(a) $\alpha = 0.25$ (b) $\alpha = 0.5$ (c) $\alpha = 0.75$

Figure 17: Comparison of the band structures with different alpha values

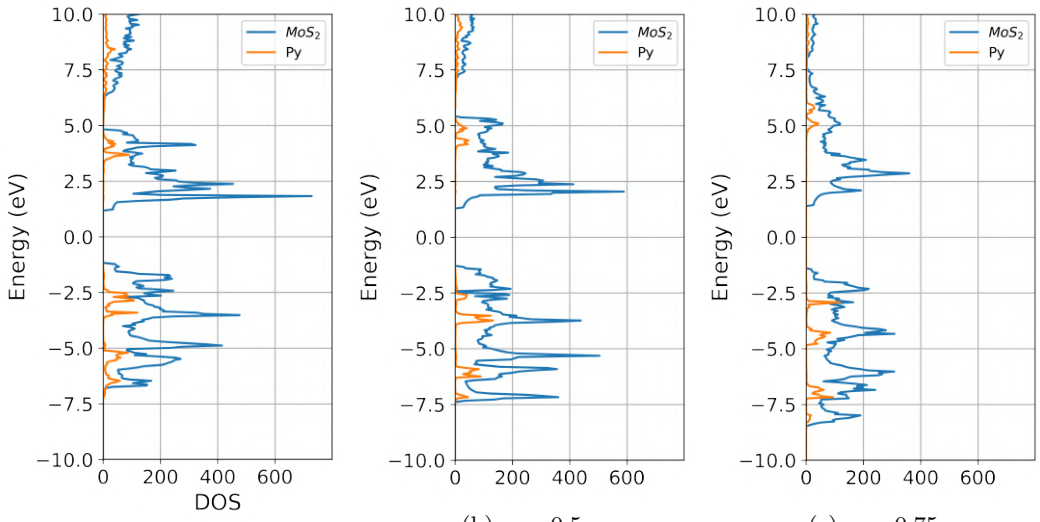

(a) $\alpha = 0.25$ (b) $\alpha = 0.5$ (c) $\alpha = 0.75$

Figure 18: Comparison of the DOS for different alpha values

4.6 Computational efficiency of the HSE method

4.6.1 Convergence time

One important interest of HSE hybrid functionals is to provide a precise computation that takes into account the Hartree-Fock exact exchange energy, and improve the computational cost compared to a PBE0 hybrid functional[21]. The different computations of MoS2 + Pyridine were performed on using the same conditions and parameters (number of processors, number of empty states, k-grid, ...). As we can see on figure figure.19, the computational time is only slightly diminished for $\omega = 0.11a_0^{-1}$ but nothing significant, and increased for smaller or bigger values of ω compared to the PBE0 computation, it seems that the HSE functional does not provide any kind of computational improvement, and we try to understand the reasons.
It is said in the original HSE

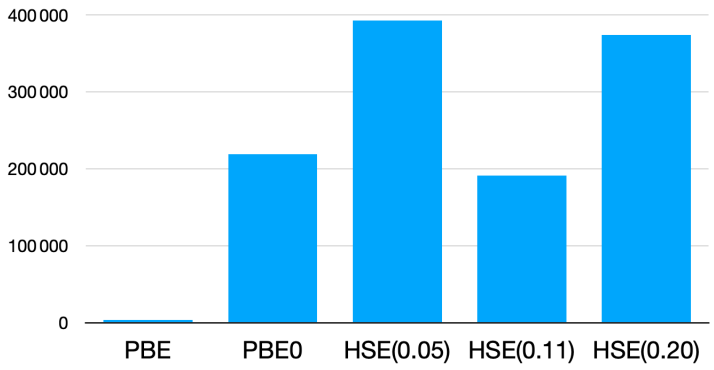

Figure 19: Computational times (in second) of pyridine @ MoS_2 for different functionals

It seems that although the HSE does not improve the computation time, it should provide a higher convergence relative to the grid size[18], however, for our system, we can not take a smaller k-grid than 3x3x1 if we want K to be a part of the grid.

5 Outlook

In this section, we comment on ideas that have not been completed, or that could be interesting to follow for better understanding of HIOS MoS_2 /pyridine,pyrene structures, beyond the functionals.

5.1 Band unfolding

5.1.1 Purpose and Principle

As mentioned previously, when computing crystalline supercells, the obtained band structure is a folding of the band structure of a primitive cell (fig.21), this can be annoying, because as in the case of 3x3MoS_2, the band gap would be localized on the wrong point of the reciprocal space. And more generally, a lot of bands would be associated to incorrect wave vectors.

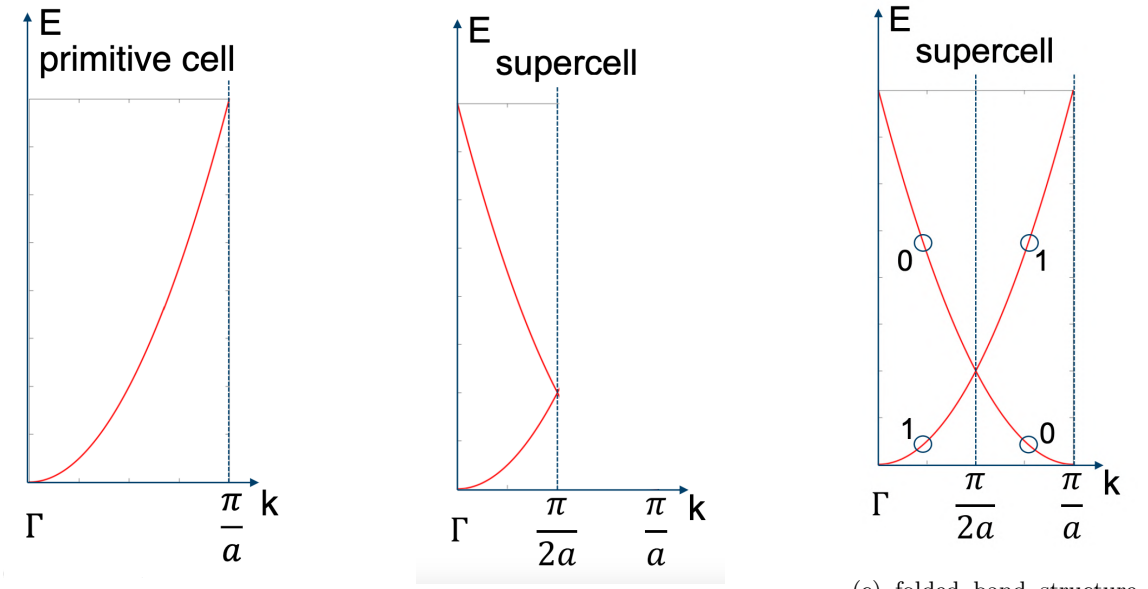

(a) primitive cell band structure

(b) 2x folded band structure

(c) folded band structure with its attributed weights to come back to the primitive cell

Figure 20: Simplified representation of band folding and unfolding process[20]

For those reasons, it is interesting to develop a so-called "band-unfolding" post processing program, that unfolds the band structure back to the primitive one. There are different methods, but the principle remains to attribute to each k-point of each band a spectral weight (from 0 to 1) fig.20.

5.1.2 Projection method

The set of **G** vectors lattice of the supercell in the reciprocal space is linked to the set of **g** vectors lattice of the primitive cell by $\mathbf{G} = M^{-1}\mathbf{g}$ with M the transformation matrix in the real space. For every **k** in the primitive Brilliouin zone (pbz), there exists a unique $K = k - G_0$ wave vector in the Supercell Brilliouin zone (SBZ) where $G_0 = \sum_i G_i$, **k** is said to fold in **K**. Inversely, **K** unfolds into a set of $\mathbf{k}_i$ vectors $\mathbf{k}_i = \mathbf{K} + G_i, i = 1, ..., N_k$ with $N_k = det(m)$ the number of SBZ contained into the pbz[**?**].

Each SC eigenvector $|\mathbf{K}m\rangle$ can be expressed as a linear combination of SC eigenvectors : $|\mathbf{K}m\rangle = \sum_{i=1} \sum_n F(\mathbf{k}_i, n, \mathbf{K}, m) \, |\mathbf{k}_i n\rangle$ with m and n the band indices. The purpose of the procedure is to get the PC eigenstates $|\mathbf{k}_i n\rangle$ from the SC calculation. for that we obtain their contribution $F(\mathbf{k}_i, n, \mathbf{K}, m)$ by projecting

$$P_{\mathbf{K}m}(\mathbf{k}_i) = \sum_n | \langle \mathbf{K}m | \mathbf{k}_i n \rangle |^2 \tag{17}$$

this gives the probability of finding a set of PC states $|\mathbf{k}_i n\rangle$ contributing to the SC state $|\mathbf{k}m\rangle$, from

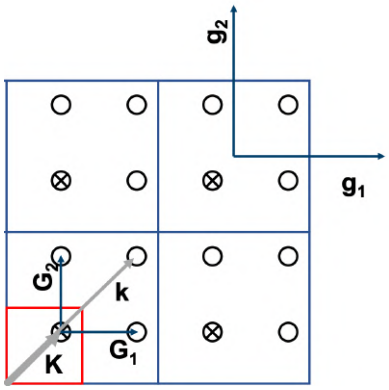

Figure 21: Schematic representation of a 2x2 supercell reciprocal lattice with the **k** folded into **K** represented [20]

that, we can easily obtain the Spectral function of continuous variable E :

$$A(\mathbf{k}_i, E) = \sum_m P_{\mathbf{K}m}(\mathbf{k}_i)\delta(E_m - E) \tag{18}$$

Problems of implementation : To compute the projections $\langle \mathbf{K}m|\mathbf{k}_i n\rangle$, we need to use :

$$P_{\mathbf{K}m}(\mathbf{k}) = \sum_{\tilde{\mathbf{G}}(\mathbf{k})} \sum_{\mathbf{G'}} C^*_{n,\mathbf{K}(\mathbf{k})}(\mathbf{G}(\mathbf{k})) \cdot C_{n,\mathbf{K}(\mathbf{k})}(\mathbf{G'}) \cdot S_{\mathbf{K}(\mathbf{k}),\tilde{\mathbf{G}}(\mathbf{k}),\mathbf{G}'} \tag{19}$$

with $\tilde{\mathbf{G}}$ the subset of G matching to one **k** and its multiples in the unit cell. $C_{n,\mathbf{k}}(\mathbf{G})$ the expansion coefficients, and $S_{\mathbf{k},\mathbf{G},\mathbf{G}'}$ the overlap matrix.
Which means we had to compute overlap matrices for each k-point, thus, the calculation of the spectral function could not be made truly in post processing, and had to be calculated at the same time as the bandstructure. However, we had to face a problem, because in the `exciting` code, the eigenvalues are stacked on top of each other so that bands never intersect, which means the bands stored in the output files do not correspond to the "physical" bands, so we tried to go deeper under the hood to find a way to produce overlap matrices with matching band indices, but could not mostly by lack of time.
We then tried an approximation method where we used a simplified "all plane wave method" where the overlap matrix is considered as a plane wave overlap matrix (easy to simplify analytically), but as expected, it provided wrong results for most of the bands because the basis set was inappropriate. To experiment this method (and the next one), we decided to perform on simple 2x2 graphene supercell because it is a material with with very distinguishable bands, for simplicity we only evaluated the density of states in Γ, the expected k-band weights in Γ, respectively for each of the thirteen firsts bands are shown in table 6.

5.1.3 Method of local density of states

This method[] is made to be simpler than the previous one, and does not require a computation over the neighboring bands, and thus should not be a problem to implement. The idea is simply to

Table 6: Tab of the obtained weights for band unfolding of a 2x2 graphene supercell in Gamma, the first line gives the band index (from lowest to highest energy), the second line gives the ideal value that should be reached, the third line provides the results obtained by the projection method using the plane wave approximation matrix, and the last line gives the results obtained with the local density method

index	1	2	3	4	5	6	7	8	9	10	11	12	13
Theoretical	1	0	0	0	0	0	0	1	0	0	1	1	0
Projection	1.1	0.97	0.76	0.75	0.47	0.03	0.11	95	0.32	0.77	0.96	0.78	0.42
lDOS	1.0	0.64	0.42	0.56	0.54	0.76	0.6	0.98	0.74	0.43	0.95	0.89	0.2

compute the local density of states.

$$n(q,\epsilon) = \sum_i \int_{SBZ} d\mathbf{K} |\psi_{\mathbf{K},i}(\mathbf{q})|^2 \delta(\epsilon - \epsilon_{\mathbf{K},i}) = \sum_i |u_{\mathbf{K}_q,i}| \tag{20}$$

We found only one occurence of this method being used, and the provided results had a lot of artifacts, and does not seem appropriate for an important number of overlapping bands. And our application did not show satisfying results (table.6).

5.2 GW approximation

The `exciting` code has a GW approximation module implemented[1], it solves the linearized quasi-particle equation[19] that introduces the energy dependance of the self energy $\Sigma = G_0W_0$ with G_0 the non interacting single-particle Green function computed from the KS states and W_0 is the screened Coulomb interaction, offering first order perturbative corrections. It would be very interesting to see how the GW corrects the KS states obtained with the different functionals as the GW approach is considered the state of the art when it comes to electronic band structures[5]. When obtained in non-self-consistency ($G0W0$), they likely depend on the underlying DFT density and hybrid functionals are closer to the final result[5]. Unfortunately, by lack of time, the convergence tests for those computations could not be achieved.

5.3 Exciton study

The `exciting` code provides (as the name suggests), post processing tools to solve the Bethe-Salpeter equation and even visualize excitons, It could help us anticipate the presence of charge-transfer electrons for optoelectronics application, as well as consider the dielectric function of our materials.

6 Conclusion

This work has been dedicated to the theoretical investigations of the electronic properties of heterostructures made of MoS_2 and adsorbed pyridine and pyrene molecules. With this intent, a DFT combined with GGA method was the first choice. For more accurate results, the hybrid functionals HSE and PBE0 were used as they have proven to give better results (than GGA) for each component of the studied heterostructures, and they are common methods for other types of heterojunctions to compute e.g. bandgaps, and band offsets.
The analysis of these computations tell us that monolayer MoS_2 is a candidate substrate for different kind of ultra thin optoelectronic devices. As its strong carrier mobility coupled with strongly light interacting molecules can lead to different types of level alignment. A heterostructure with pyridine gives a type-I alignment which makes it an interesting material for light emitting devices in the visible spectrum. On the other hand, a heterostructure with adsorbed pyrene yields a type-II alignment as pyrene is a strong donor, which makes it suitable for light harvesting applications. As the offsets obtained with the hybrid functionals were around 0.7 eV for pyrene @ MoS_2 and 1.2 eV for the pyridine @ MoS_2 which is higher than the usual offset precision of HSE, we can be confident with the type alignment predicted.
As a further step, it would be very interesting to use the GW approach to confirm our previous conclusions. The reason for this is that band alignment requires precise quantitative results, and GW is the state of the art in this respect. Further investigations for optoelectronic properties could be made by solving the BSE starting with the electronic structure obtained with GW.This would allow for studying e.g. charge-transfer electrons

References

[1] Christian Meisenbichler Dmitrii Nabok Pasquale Pavone Santiago Rigamonti Stephan Sagmeister-Ute Werner1and Claudia Draxl Andris Gulans, Stefan Kontur. *exciting: a full-potential all-electron package implementing density-functional theory andmany-body perturbation theory. J. Phys.: Condens. Matter 26 363202*, 2014.

[2] J. Brivio V. Giacometti A. Kis B. Radisavljevic, A. Radenovic. *Single-layer MoS2 transistors. Nature Nanotechnology volume 6, pages147–150*, 2011.

[3] Xinfeng Liu Bo Liu Xiao Liang Lei Bi Longjiang Deng-Tze Chien Sum Bo Peng, Guannan Yu and Kian Ping Loh. *Ultrafast charge transfer in MoS2/WSe2 p–n Heterojunction. 2D Mater. 3 025020*, 2016.

[4] John P. Perdew; Matthias Ernzerhof; Kieron Burke. *Rationale for mixing exact exchange with density functional approximations. J. Chem. Phys. 105 (22): 9982–9985*, 1996.

[5] Karsten Hannewald Claudia Draxl, Dmitrii Nabok. *Organic/inorganic Hibrid Materials: Challenges for ab initio Methodology. Acc. Chem. Res. 2014, 47, 11, 3225–3232*, 2014.

[6] L. A. Cole and J. P. Perdew. *Calculated electron affinities of the elements. Phys. Rev. A. 25 (3): 1265–1271*, 1982.

[7] L. WestonH. TailorK. KrishnaswamyL. BjaalieC.G. Van de Walle. Accurate and efficient band-offset calculations from density functional theory. *computational Materials Science 151*, 2018.

[8] Yang Cao Dongcheng Chen, Shi-Jian Su. *Nitrogen Heterocycle-Containing Materials for Highly Efficient Phosphorescent OLEDs with Low Operating Voltage. Journal of Materials Chemistry C 2(45)*, 2014.

[9] A. R. Klots et al. *Probing excitonic states in suspended two-dimensional semiconductors by photocurrent spectroscopy. SCIENTIFICREPORTS 4 : 6608*, 2014.

[10] Dariusz W. Szczepanik et al. *The Role of the Long-Range Exchange Corrections in theDescription of Electron Delocalization in Aromatic Species. Journal of Computational Chemistry 38(16)*, 2017.

[11] Debora Pierucci et Al. *Large area molybdenum disulphide- epitaxial graphene vertical Van der Waals heterostructures. Scientific Reports 6(1):26656*, 2016.

[12] E. S. Kadantsev et al. Electronic structure of a single mos2 monolayer. *Sol State Commun., 152, 909–913*, 2012.

[13] Mikhail A Filatov et al. *BODIPY-Pyrene and Perylene Dyads as Heavy-Atom-Free Singlet Oxygen Sensitizers. ChemPhotoChem 2(7):606-615*, 2018.

[14] Nengjie Huo et al. *High carrier mobility in monolayer CVD-grown MoS2 through phonon suppression. nanoscale issue 31*, 2018.

[15] S. Kurth et al. Density-functional theory. *Encyclopedia of Condensed Matter Physics*, 2005.

[16] Shuji Ogata et al. Multi-thousand-atom dft simulation of li-ion transfer through the boundary between the solid–electrolyte interface and liquid electrolyte in a li-ion battery. *J. Phys. Chem. C 2013, 117, 35, 17960–17968*, 2013.

[17] Kyoung Chul Ko Jin Yong Lee Francesc Viñes, Oriol Lamiel-García and Francesc Illas. *Systematic study of the effect of HSE functional internal parameters on the electronic structure and band gap of a representative set of metal oxides. Journal of computational chemistry*, 2017.

[18] Jochen Heyd and Gustavo E. Scuseria. *Efficient hybrid density functional calculations in solids: Assessment of the Heyd–Scuseria–Ernzerhof screened Coulomb hybrid functional. J. Chem. Phys. 121, 1187*, 2004.

[19] M. S. Hybertsen and S. G. Louie. *Phys. Rev. B 34, 5390*, 1986.

[20] Peter Grünberg Institut. Forschungszentrum jülich and jara, 52425 jülich, germany. , 2019.

[21] Gustavo E. Scuseria Jochen Heyd and Matthias Ernzerhof. *Hybrid functionals based on a screened Coulomb potential. J. Chem. Phys. 118*, 2003.

[22] jynto. https://commons.wikimedia.org/wiki/file:pyrene$_m olecule_f rom_x tal_b all.png.$, 2017.

[23] S. Sharma K. Dewhurst. Development of the elk lapw code. *Max planck institut of microstructure physics*, 2021.

[24] Ryan D. Dolewski Michael C. Hilton and Andrew McNally. Selective functionalization of pyridines via heterocyclic phosphonium salts. *J. Am. Chem. Soc. 2016, 138, 42, 13806–13809*, 2016.

[25] Micael J. T. Oliveira Lucia Reining Miguel A. L. Marques, Julien Vidal and Silvana Botti. *Density-based mixing parameter for hybrid functionals. PHYSICAL REVIEW B 83, 035119* , 2011.

[26] Ben Mills. https://commons.wikimedia.org/wiki/file:pyridine-crc-mw-3d-balls.png. , 2009.

[27] Andris Gulans Caterina Cocchi Olga Turkina, Dmitrii Nabok and Claudia Draxl. *Electronic and Optical Excitations at the Pyridine/ZnO(1010) Hybrid Interface. Adv. Theory Simul. 2019, 2, 1800108*, 1996.

[28] Dobrowolski Jan C Ozimiński, Wojciech P. - and -electron contributions to the substituent effect: natural population analysis. *Journal of Physical Organic Chemistry. 22 (8): 769–778*, 2009.

[29] J. P. Perdew and A. Zunger. *Self-interaction correction to density-functional approximations for many-electron systems. Phys. Rev. B. 23 (10): 5048–5079*, 1981.

[30] F. Reyes-Retana, J.A.; Cervantes-Sodi. Spin-orbital effects in metal-dichalcogenide semiconducting monolayers. *Scientific Reports. 6: 24093*, 2016.

[31] L. Wilk S. H. Vosko and M. Nusair. *"Accurate spin-dependent electron liquid correlation energies for local spin density calculations: a critical analysis". Can. J. Phys. 58 (8): 1200–1211*, 1980.

[32] Akira Yamamoto Shimpei Naniwa, Akanksha Tyagi and Hisao Yoshida. *Visible-light photoexcitation of pyridine surface complex, leading to selective dehydrogenative cross-coupling with cyclohexane. Physical Chemistry, Chemical Physics issue 45*, 2018.

[33] Christopher P.; Bittencourt Carla; Arenal Raul; Pelaez-Fernandez Mario; Sayed-Ahmad-Baraza Yuman; Canton-Vitoria Ruben Tagmatarchis, Nikos; Ewels. *"Functionalization of MoS 2 with 1,2-dithiolanes: toward donor-acceptor nanohybrids for energy conversion". NPJ 2D Materials and Applications. 1 (1): 13.* , 2017.

[34] Qing Tang and De en Jiang. Stabilization and band-gap tuning of the 1t-mos2 monolayer by covalent functionalization. *Chem. Mater. 2015, 27, 37433748*, 2015.

[35] C.D.Karp V.Glushko, M.S.R.Thaler. *Pyrene fluorescence fine structure as a polarity probe of hydrophobic regions: Behavior in model solvents. Archives of Biochemistry and Biophysics Volume 210, Issue 1, August 1981, Pages 33-42*, 1981.